




Multiple Brillouin Zone Winding of Topological Chiral Edge States for Slow Light Applications

Fujia Chen,^{1,2,3,4,*} Haoran Xue,^{5,*} Yuang Pan,^{1,2,3,4} Maoren Wang,⁶ Yuanhang Hu,⁶ Li Zhang,^{1,2,3,4} Qiaolu Chen,^{1,2,3,4}
 Song Han ^{1,2,3,4} Gui-geng Liu,^{7,8} Zhen Gao ⁹ Peiheng Zhou,^{6,†} Wenyan Yin,^{1,‡} Hongsheng Chen,^{1,2,3,4,§}
 Baile Zhang,^{7,8,||} and Yihao Yang ^{1,2,3,4,¶}

¹*State Key Laboratory of Extreme Photonics and Instrumentation, ZJU-Hangzhou Global Scientific and Technological Innovation Center, Zhejiang University, Hangzhou 310027, China*

²*International Joint Innovation Center, The Electromagnetics Academy at Zhejiang University, Zhejiang University, Haining 314400, China*

³*Key Lab. of Advanced Micro/Nano Electronic Devices & Smart Systems of Zhejiang, Jinhua Institute of Zhejiang University, Zhejiang University, Jinhua 321099, China*

⁴*Shaoxing Institute of Zhejiang University, Zhejiang University, Shaoxing 312000, China*

⁵*Department of Physics, The Chinese University of Hong Kong, Shatin, Hong Kong SAR, China*

⁶*Key Laboratory of Multi-spectral Absorbing Materials and Structures of Ministry of Education, University of Electronic Science and Technology of China, Chengdu 611731, China*

⁷*Division of Physics and Applied Physics, School of Physical and Mathematical Sciences, Nanyang Technological University, 21 Nanyang Link, Singapore 637371, Singapore*

⁸*Centre for Disruptive Photonic Technologies, The Photonics Institute, Nanyang Technological University, 50 Nanyang Avenue, Singapore 639798, Singapore*

⁹*Department of Electrical and Electronic Engineering, Southern University of Science and Technology, Shenzhen 518055, China*



(Received 5 January 2023; accepted 29 February 2024; published 11 April 2024)

Photonic Chern insulators are known for their topological chiral edge states (CESs), whose absolute existence is determined by the bulk band topology, but concrete dispersion can be engineered to exhibit various properties. For example, the previous theory suggested that the edge dispersion can wind many times around the Brillouin zone to slow down light, which can potentially overcome fundamental limitations in conventional slow-light devices: narrow bandwidth and keen sensitivity to fabrication imperfection. Here, we report the first experimental demonstration of this idea, achieved by coupling CESs with resonance-induced nearly flat bands. We show that the backscattering-immune hybridized CESs are significantly slowed down over a relatively broad bandwidth. Our work thus paves an avenue to broadband topological slow-light devices.

DOI: [10.1103/PhysRevLett.132.156602](https://doi.org/10.1103/PhysRevLett.132.156602)

Recent years have witnessed the rapid development of photonic topological insulators in time-reversal-breaking systems, which prohibit light propagation in bulk but can sustain topologically protected photonic chiral states at edges, which are intrinsically immune to backscattering and Anderson localization caused by the disorder [1–11]. The existence of these robust chiral edge states (CESs) is guaranteed by the nonzero Chern number of the bulk, according to the principle of bulk-edge correspondence [12]. However, the concrete edge dispersion can be engineered to exhibit various properties, whose full potential has not been unleashed.

When passing through certain media, light can be slowed down with a group velocity remarkably lower than that in free space [13–15]. This slow-light effect can dramatically enhance light-matter interaction and significantly minimize the photonic device footprint, enabling numerous photonic applications in switching, storage, buffers, and quantum optics [16–20]. Conventional slow-light devices have

regrettably suffered from two fundamental limitations: (1) a very low group velocity implies keen sensitivity to disorders from inevitable fabrication imperfections in practice, leading to significant loss arising from backscattering and Anderson localization [21–23]; (2) the reduced group velocity usually comes at the expense of bandwidth, resulting in the narrowband operation that is highly undesirable in a wide range of applications [19,20].

Only recently has it been suggested theoretically that the aforementioned limitations can be potentially overcome by exploiting the multiple winding of the topological CESs around the Brillouin zone (BZ) in a time-reversal-breaking photonic system [24–26]. Over a maintained bandwidth, the engineered CESs can have significantly reduced group velocity with small variation, which is inversely proportional to the winding number. This thus provides a work-around to the bandwidth-group velocity trade-off. Note that the operational bandwidth should not be greater than the topological band gap width. To achieve the multiple

winding of the CESs requires judicious engineering of topological edge states that have been rarely explored compared to the extensive study of bulk states. There have been two theoretical proposals to achieve multiple BZ winding of the CESs for broadband topological slow light. The first is to engineer the nearest-neighbor and next-nearest-neighbor couplings in a modified Haldane model, whose design has not yet been translated into a realistic photonic setting [24]. The second is to load judiciously designed resonators at the edge termination of a photonic Chern insulator (PCI) [25,26]. As a result, the CESs couple with the nearly flat bands (NFBs) induced by resonance modes to produce hybridized CESs that wind around the BZ multiple times. So far, neither type of BZ winding of CESs has been explored experimentally.

Here, we report the experimental demonstration of the multiple BZ winding of topological CESs to slow down light over a relatively wide range of frequencies. We experimentally show that by coupling to the resonance-induced NFBs, the CESs can wrap many times around the BZ. Thus, their group velocity can be significantly slowed down, and the fractional bandwidth with a reduction of the group velocity of more than 50% relative to the original CESs is 5.7%. Impressively, the winding number can be up to five in experiments and has no strict limit in theory. Finally, we demonstrate the robustness of such broadband topological slow light against obstacles and defects, as well as the smooth transport through slow-light regions with different group velocities.

Figures 1(a) and 1(b) show the experimental setup. The PCI consists of a square lattice of magnetically biased yttrium-iron-garnet (YIG) rods [27] with lattice constant $a = 14.6$ mm and radius $d = 4.4$ mm. In this work, we focus on the transverse electric (TE) modes with electric fields polarized along the YIG rods. Several YIG rods are enclosed by gratings of metal cylinders to construct photonic cavities that are periodically loaded at the edge of the PCI. As the distance between adjacent metal cylinders ($\delta = a/3$) is much smaller than the cut-off wavelength ($\lambda_0/2$, with λ_0 the operating wavelength) for TE modes, the metal gratings behave approximately as metal walls [27,29]. The resonance modes in cavities are determined by the cavity width Λ ($\Lambda = 2a$ in our designs) and the cavity depth D [$D = 2a$ in Figs. 1(a) and 1(b)]. The gap width g [$g = 4\delta$ in Figs. 1(a) and 1(b)] controls the coupling strength between the CESs and the resonance modes. All YIG rods are placed in an air-loaded waveguide composed of two parallel copper plates and magnetized by small permanent magnets located at the top and bottom of each YIG rod [27]. Note that a square array of small holes, with a diameter of 2 mm and a period of $a/3$, are drilled through the top copper plate for inserting metal cylinders and probes. Figure 1(c) shows the numerically calculated band structure of the PCI. Under a z -oriented external static magnetic field with $B = 0.043$ Tesla, there is a Chern-type band gap from 11.5 to 12.9 GHz with a gap Chern number $C_{\text{gap}} = 1$ [27].

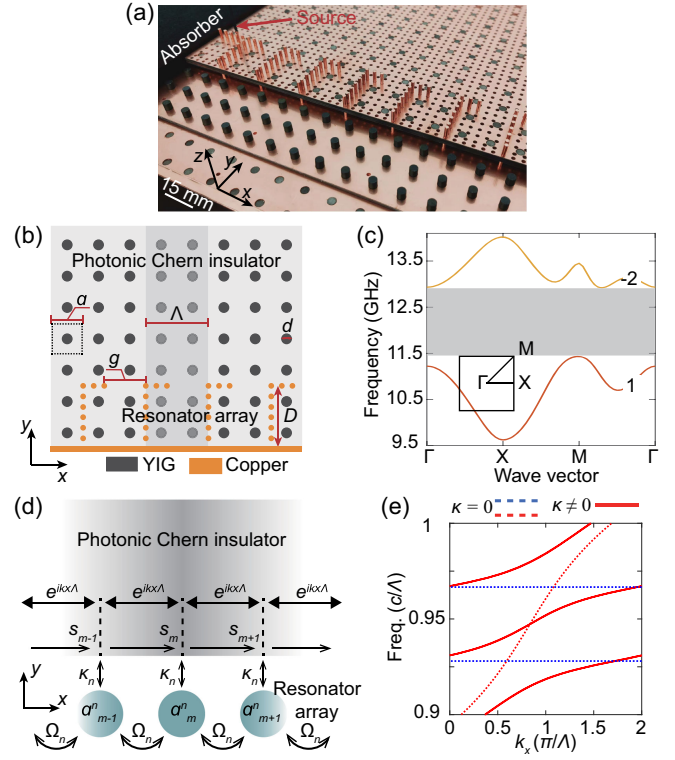


FIG. 1. Experimental setup and schematic. (a),(b) Photograph and diagram of the experimental setup. The lattice constant $a = 14.6$ mm. The red arrow in (a) shows the position of the source antenna. The dashed box in (b) indicates the unit cell of the PCI. The gray circles in (b) represent YIG cylinders with a diameter $d = 4.4$ mm. The yellow parts represent copper. Here, g , D , and Λ denote the gap width, the cavity depth, and the cavity width, respectively. (c) Second and third bands of the PCI under an external magnetic field. The gray rectangle indicates the topological band gap. The Chern number of each band is labeled. The first band not shown here is trivial. The inset shows the BZ. (d) CMT model. (e) Calculated dispersions in the decoupling (i.e., $\kappa = 0$, the dashed curves) and coupling (i.e., $\kappa \neq 0$, the solid curves) regimes. The blue and red dashed curves represent the NFBs and the CESs, respectively. The detailed parameters can be found in [27].

The experimental setup in Fig. 1(a) can be understood from the schematic in Fig. 1(d). The resonators, periodically arranged at the bottom edge of a PCI, are isolated from each other and coupled to the CESs with a strength κ . When $\kappa = 0$, the PCI is equivalently terminated with a perfect electric conductor (PEC) wall. For a typical PCI with $|C_{\text{gap}}| = 1$, a single edge dispersion traverses the entire band gap [2,3]. Because of the decoupling, the crossing points between the CES dispersion and the NFBs of the resonator array are preserved. When $\kappa \neq 0$, the CESs couple to the resonator modes, splitting up the crossing points. The resulting hybridized edge states are still chiral, and the corresponding dispersion crosses the entire topological band gap [see Fig. 1(e)]. Compared with the original CESs, the hybridized CESs exhibit dispersion

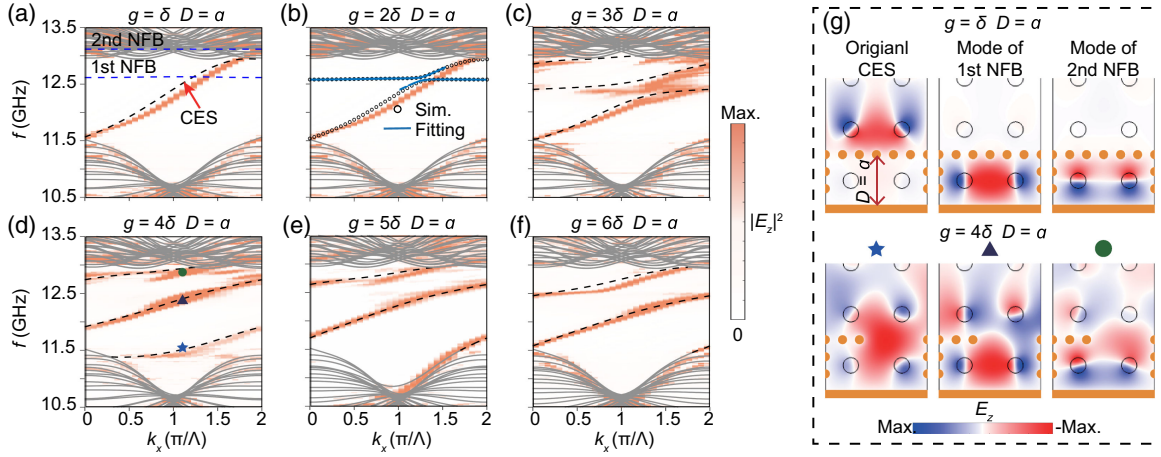


FIG. 2. Coupling between the CESs and the NFBs. (a)–(f) Measured (color) and simulated edge dispersions (black dashed curves) for different g varying from δ to 6δ . In all cases, $D = a$. The blue dashed curves denote the NFBs. The gray curves represent projected bulk states. The color bar represents the momentum-space energy intensity of the measured electric field. The cyan solid curves in (b) represent the fitted dispersion with CMT. (g) Simulated eigenmode profiles (E_z) of the edge states for the cases without (top panel) and with coupling (bottom panel). The frequency of each mode can be found in (a) and (d).

wrapping multiple times around the BZ. The group velocity of the hybridized CESs, defined as the slope of the dispersion curve (i.e., $v_g = d\omega/dk$, where ω and k are the angular frequency and the wave vector, respectively), is significantly slowed down, with the slowdown factor proportional to the number of NFBs available in the topological band gap.

We first experimentally investigate the coupling process between the CESs and resonance modes. Figures 2(a)–2(f) show the measured and simulated dispersions of the CESs and the NFBs. When g is very small (e.g., $g = \delta$), the evanescent coupling between the CESs and the resonance modes is negligible, and the CESs do not hybridize with the resonance modes. Correspondingly, the dispersion of CESs and NFBs induced by the weak coupling between adjacent resonators [27] intersect with each other [see Fig. 2(a)]. As the coupling strength increases, the CESs are strongly coupled to the resonance modes, forming hybridized CESs [see Fig. 2(g)]. Consequently, the crossing points are split up, and the dispersion curves of the CESs and the NFBs connect with each other to produce a single dispersion curve winding twice around the BZ in the band gap. It is obvious that the hybridized CESs exhibit much lower group velocities but the same bandwidth as the original CESs. Continuously increasing g , the coupling strength is so considerable that the NFBs shift, and so do the dispersions of hybridized CESs (see Fig. 2(d)–2(f)). In particular, at $g = 4\delta$, the second NFB shifts into the topological band gap, enabling one additional winding of the hybridized CESs [see Fig. 2(d)]. In the following, we will focus on $g = 4\delta$.

To explain the mechanism, we further establish a rigorous coupled-mode theory (CMT) [25] illustrated in Fig. 1(d). The corresponding dynamic equation is [27]

$$\frac{d}{dt} a_m^n = [-i(\omega_{0n} - 2\Omega_n \cos(k_x \Lambda)) - \gamma_n] a_m^n + \kappa_n s_m \quad (n = 1, 2, \dots, N), \quad (1)$$

where N is the number of resonance modes located in the topological band gap. a_m^n is the normalized amplitude of n th resonance mode in the m th resonator. ω_{0n} is the resonance center frequency, γ_n is the loss rate, Ω_n is the evanescent coupling rate between adjacent resonators, and $\kappa_n = \sqrt{2\gamma_n}$ is the coupling coefficient between the n th resonance mode and CESs. s_m is the normalized amplitude of CESs after propagating $(m - 1)$ resonators. s_m satisfies

$$s_{m+1} = e^{ik_x \Lambda} s_m \quad \text{and} \quad s_{m+1} = e^{ik_w \Lambda} \left(C s_m + \sum_n^N \kappa_n a_m^n \right), \quad (2)$$

where k_w is the dispersion of CESs, and C is the direct scattering rate. Combining Eqs. (1) and (2) with Bloch's theorem and CMT identities, we arrive at an equation

$$e^{ik_x \Lambda} = e^{ik_w \Lambda} \left[1 + \sum_n^N \frac{2\gamma_n}{i(\omega - \omega_{0n} + 2\Omega_n \cos(k_x \Lambda)) - \gamma_n} \right], \quad (3)$$

which describes the dispersions of hybridized CESs. We take $g = 2\delta$ as an example. By fitting the simulated dispersion with Eq. (3), we can get the coupling rate between the resonance mode and the CESs, $\kappa_1 = 0.062$ GHz, and the coupling rate between adjacent resonators, $\Omega_1 = -0.0037$ GHz, which indicates Ω_1 is a small but non-negligible value, resulting in the NFB.

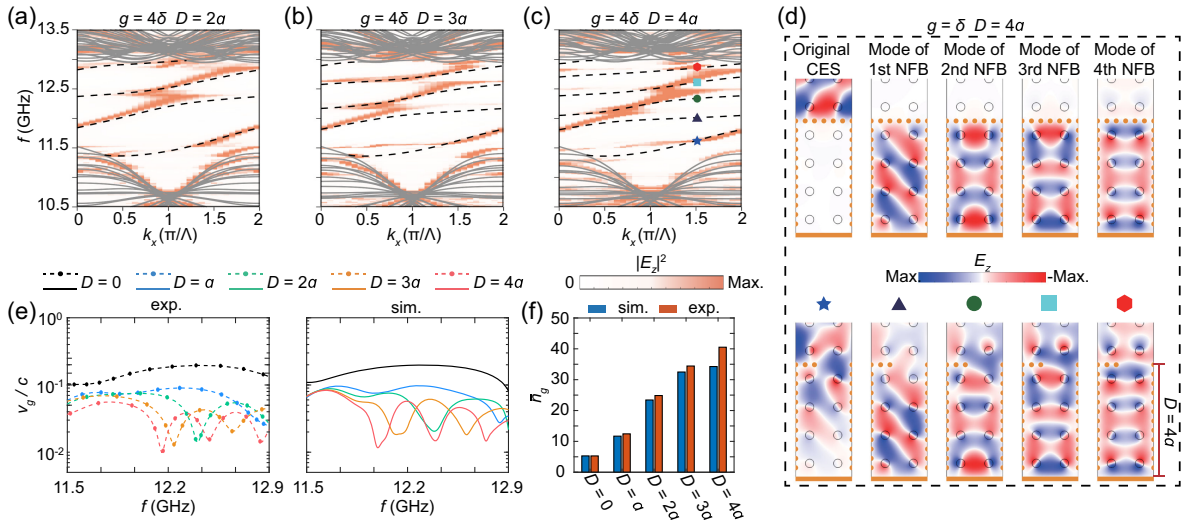


FIG. 3. Experimental observation of the broadband topological slow light through higher BZ winding. (a)–(c) Measured (color) and simulated (black dashed curves) edge dispersions for $D = 2a$ (a), $3a$ (b), and $4a$ (c), respectively. The solid gray curves represent projected bulk states. (d) Simulated eigenmode profiles (E_z) of edge states without (left panel) and with (right panel) coupling. The frequency of each mode in the coupling (decoupling) regime can be found in (c) [Fig. S4(a)]. (e),(f) Retrieved group velocities (e) and average group indices (f) from the measured and simulated dispersions of the hybridized CESs for different values of D .

We then perform experiments to demonstrate the broadband topological slow light through the higher momentum-space winding by increasing the cavity depth D . Figures 3(a)–3(c) show the measured and simulated edge dispersions for $D = 2a$, $3a$, and $4a$, respectively. When D increases, the dispersions of the hybridized CESs wrap more times around the BZ. Since the bandwidth of the topological band gap remains unchanged, the increases in winding numbers lead to the reduction in the group velocities, enabling the broadband topological slow light. Note that due to the impedance mismatch between the measurement system and the hybridized CESs, some edge states are weakly excited, which leads to the nonuniform brightness of the measured band structures.

The higher BZ winding achieved here stems from the increment of NFBs determined by the cavity size. Taking $D = 4a$ as an instance, there are four NFBs within the band gap coupling with the CESs and forming new hybridized CESs [see Fig. 3(d)]. Interestingly, these hybridized CESs exhibit completely different mode profiles but lie on the same band. One can imagine that as the edge dispersion winds around the BZ, the edge modes evolve from one type to another.

To quantitatively characterize our broadband topological slow-light systems, we retrieve the group velocities of the hybridized CESs [see Fig. 3(e)]. One can see that a higher winding results in a significant reduction of the group velocities for the most frequencies in the topological band gap. Remarkably, the group velocities are always positive within the band gap, i.e., the dispersion curve is monotonical, which means the unidirectional propagation of modes. We further calculate the average group index (i.e., the

slowdown factor) of the hybridized CESs, defined as

$$\bar{n}_g = \int_{f_a}^{f_b} n_g(f) df / \Delta f, \quad (4)$$

where $\Delta f = f_b - f_a$ ($f_a = 12$ GHz, $f_b = 12.7$ GHz) is the frequency range (the fractional bandwidth of 5.7%) in which the reduction of a group velocity is more than 50% relative to the original CESs. $n_g(f) = c/v_g$ is the group index, and c is the light speed in the vacuum. The measured averaged slowdown factors increase remarkably 7.8 times from 5.28 to 40.53 when D varies from 0 to $4a$ [see Fig. 3(f)]. The slowdown factor can be further boosted by increasing D and has no strict limit in principle. As for the frequency dispersion of group velocity, it can be moderated by further optimizations [27].

Finally, we experimentally show the robustness of the broadband topological slow light against disorder, another property that is fundamentally distinct from the conventional slow-light approaches. In experiments, we introduce two types of disorders into our system by removing several YIG rods around the edge [see Figs. 4(a) and 4(b)], and inserting a large PEC pillar into the edge [see Figs. 4(c) and 4(d)], respectively. In both cases, only the forward transmission characterized by S_{21} is allowed, and the backward transmission characterized by S_{12} is forbidden, within the topological band gap. The robustness of the hybridized CESs can also be manifested from the simulated field distributions, where the hybridized CESs can pass through obstacles and propagate unidirectionally without suffering from backscattering. Remarkably, we also experimentally show that in sharp contrast to the conventional slow-light

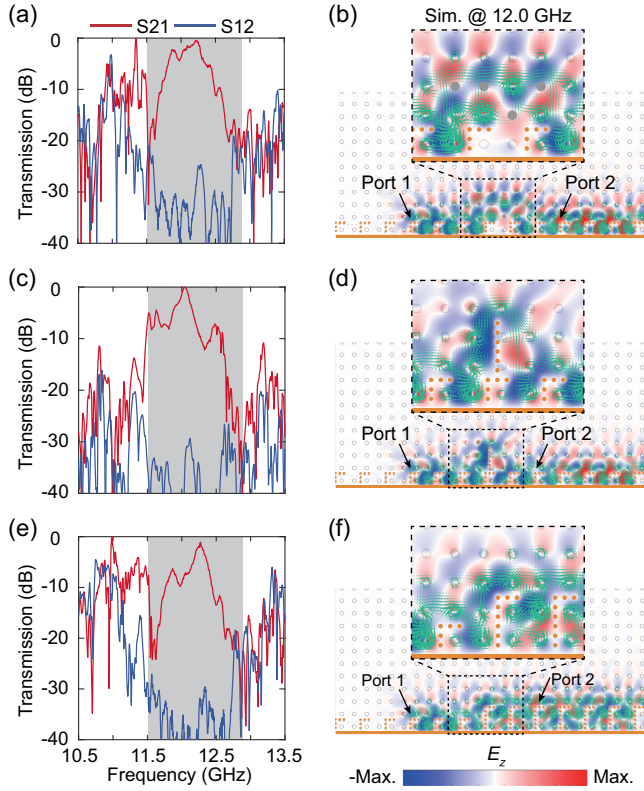


FIG. 4. Demonstration of the robustness of the broadband topological slow light. (a),(b) Measured transmission (a) and simulated E_z field and energy flux distributions (b) when four YIG pillars are removed. The gray circles in (b) represent removed YIG. (c),(d) Measured transmission (c) and simulated E_z field and energy flux distributions (d) when the edge is blocked by a large PEC obstacle. (e),(f) Measured transmissions (e) and simulated E_z field and energy flux distributions (f) when the hybridized CESs pass through an interface between two regions with different group velocities. The left (right) region has $D = a$ ($D = 2a$). The S_{21} (S_{12}) parameter is measured by placing the source at port 1 (port 2) and the detector at port 2 (port 1), as indicated by black arrows.

systems that require cautious designs to reduce the reflection losses at the interfaces between two regions with different slowdown factors, our topological slow-light system can automatically exhibit complete transmission at those interfaces over a broad frequency range, regardless of the interface details and the group velocities at two interfaced regions [see Figs. 4(e) and 4(f)]. Besides, it is worth mentioning that the topological slow light is also robust against the detuning of resonators' frequencies [27].

We have thus experimentally demonstrated the higher BZ winding of CESs for slow light applications. We show that by coupling the CESs to the resonance-induced NFBs, the dispersions of the hybridized CESs can wind many times around the BZ, and the corresponding group velocities can be significantly reduced over a relatively broad operational bandwidth. Our approach, therefore, simultaneously overcomes the limitations of narrow bandwidths

and susceptibility to disorders caused by fabrication imperfections. It is worth noting that the topological slow light in time-reversal-symmetric photonic topological insulators can still be backscattered by disorders that do not preserve certain symmetries [30], which highlights the importance of the current approach in the nonreciprocal PCIs with broken time-reversal symmetry.

In terms of applications, our findings can potentially be used to enhance light-matter interactions at lower frequencies (microwave or terahertz), where gyrotropic materials are generally available [3,31,32], for both classical and quantum applications [33]. Moreover, the multiple BZ winding approach, which requires time-reversal-symmetry breaking [24–26,30], can also be generalized to higher frequencies (infrared or optics) using nonlinear photonic crystals [34], temporally modulated coupled ring resonators [35], or gyrotropic materials [6], enabling photonic applications in various scenarios, such as quantum memories and photon blockade [36]. Particularly, the broadband slow light may lower lasing threshold, as it can boost the Purcell enhancement over ensembles of inhomogeneously broadened emitters. Finally, our approach can extend to other wave systems, such as acoustic, elastic, and magnonic systems, opening an exciting avenue toward broadband slow-wave applications.

The work at Zhejiang University was sponsored by the Key Research and Development Program of the Ministry of Science and Technology under Grants No. 2022YFA1405200 (Y. Y.), 2022YFA1404704 (H. C.), 2022YFA1404902 (H. C.), and 2022YFA1404900 (Y. Y.), the National Natural Science Foundation of China (NNSFC) under Grants No. 62175215 (Y. Y.), No. 62071418 (W. Y.), and No. 61975176 (H. C.), the Fundamental Research Funds for the Central Universities (2021FZZX001-19) (Y. Y.), the Excellent Young Scientists Fund Program (Overseas) of China (Y. Y.), and the Key Research and Development Program of Zhejiang Province under Grant No. 2022C01036 (H. C.). The work at NTU was supported by the Singapore National Research Foundation Competitive Research Program under Grant No. NRF-CRP23-2019-0007 (H. X., G. g. L. and B. Z.). The work at The Chinese University of Hong Kong was supported by the start-up fund of The Chinese University of Hong Kong (H. X.).

*These authors contributed equally.

†To whom correspondence should be addressed: phzhou@uestc.edu.cn

‡To whom correspondence should be addressed: wyyin@zju.edu.cn

§To whom correspondence should be addressed: hansomchen@zju.edu.cn

||To whom correspondence should be addressed: blzhang@ntu.edu.sg

- [†]To whom correspondence should be addressed: yangyihao@zju.edu.cn
- [1] F. D. Haldane and S. Raghu, *Phys. Rev. Lett.* **100**, 013904 (2008).
- [2] Z. Wang, Y. D. Chong, J. D. Joannopoulos, and M. Soljacic, *Phys. Rev. Lett.* **100**, 013905 (2008).
- [3] Z. Wang, Y. Chong, J. D. Joannopoulos, and M. Soljacic, *Nature (London)* **461**, 772 (2009).
- [4] M. C. Rechtsman, J. M. Zeuner, Y. Plotnik, Y. Lumer, D. Podolsky, F. Dreisow, S. Nolte, M. Segev, and A. Szameit, *Nature (London)* **496**, 196 (2013).
- [5] S. A. Skirlo, L. Lu, Y. Igarashi, Q. Yan, J. Joannopoulos, and M. Soljacic, *Phys. Rev. Lett.* **115**, 253901 (2015).
- [6] B. Bahari, A. Ndao, F. Vallini, A. El Amili, Y. Fainman, and B. Kanté, *Science* **358**, 636 (2017).
- [7] G. G. Liu *et al.*, *Phys. Rev. Lett.* **125**, 133603 (2020).
- [8] G. G. Liu, P. Zhou, Y. Yang, H. Xue, X. Ren, X. Lin, H.-x. Sun, L. Bi, Y. Chong, and B. Zhang, *Nat. Commun.* **11**, 1873 (2020).
- [9] P. Zhou, G. G. Liu, X. Ren, Y. Yang, H. Xue, L. Bi, L. Deng, Y. Chong, and B. Zhang, *Light Sci. Appl.* **9**, 133 (2020).
- [10] G. G. Liu *et al.*, *Nature (London)* **609**, 925 (2022).
- [11] Y. A. Wang *et al.*, *Nat. Commun.* **14**, 4457 (2023).
- [12] T. Ozawa *et al.*, *Rev. Mod. Phys.* **91**, 015006 (2019).
- [13] L. V. Hau, S. E. Harris, Z. Dutton, and C. H. Behroozi, *Nature (London)* **397**, 594 (1999).
- [14] S. Bigelow Matthew, N. Lepeshkin Nick, and W. Boyd Robert, *Science* **301**, 200 (2003).
- [15] Y. A. Vlasov, M. O'Boyle, H. F. Hamann, and S. J. McNab, *Nature (London)* **438**, 65 (2005).
- [16] M. D. Lukin and A. Imamoglu, *Phys. Rev. Lett.* **84**, 1419 (2000).
- [17] A. V. Turukhin, V. S. Sudarshanam, M. S. Shahriar, J. A. Musser, B. S. Ham, and P. R. Hemmer, *Phys. Rev. Lett.* **88**, 023602 (2002).
- [18] F. Xia, L. Sekaric, and Y. Vlasov, *Nat. Photonics* **1**, 65 (2006).
- [19] T. Baba, *Nat. Photonics* **2**, 465 (2008).
- [20] T. F. Krauss, *Nat. Photonics* **2**, 448 (2008).
- [21] S. Hughes, L. Ramunno, J. F. Young, and J. E. Sipe, *Phys. Rev. Lett.* **94**, 033903 (2005).
- [22] R. J. Engelen, D. Mori, T. Baba, and L. Kuipers, *Phys. Rev. Lett.* **101**, 103901 (2008).
- [23] S. Mazoyer, J. P. Hugonin, and P. Lalanne, *Phys. Rev. Lett.* **103**, 063903 (2009).
- [24] J. Guglielmon and M. C. Rechtsman, *Phys. Rev. Lett.* **122**, 153904 (2019).
- [25] S. A. Mann and A. Alù, *Phys. Rev. Lett.* **127**, 123601 (2021).
- [26] L. Yu, H. Xue, and B. Zhang, *Appl. Phys. Lett.* **118**, 071102 (2021).
- [27] See Supplemental Material at <http://link.aps.org/supplemental/10.1103/PhysRevLett.132.156602> for more details on the experimental setup, topological invariant, coupled-mode theory, more NFBs, optimization of dispersion, fitting band structures, and time-domain simulations, which also includes Ref. [28].
- [28] H.-X. Wang, G.-Y. Guo, and J.-H. Jiang, *New J. Phys.* **21**, 093029 (2019).
- [29] M. Born and E. Wolf, Principles of optics: Electromagnetic theory of propagation, *Interference and Diffraction of Light*, 7th ed. (Cambridge University Press, Cambridge, United Kingdom, 1999).
- [30] C. A. Rosiek, G. Arregui, A. Vladimirova, M. Albrechtsen, B. Vosoughi Lahijani, R. E. Christiansen, and S. Stobbe, *Nat. Photonics* **17**, 386 (2023).
- [31] D. Jin, T. Christensen, M. Soljacic, N. X. Fang, L. Lu, and X. Zhang, *Phys. Rev. Lett.* **118**, 245301 (2017).
- [32] D. Wang *et al.*, *Nat. Phys.* **15**, 1150 (2019).
- [33] J. C. Owens, M. G. Panetta, B. Saxberg, G. Roberts, S. Chakram, R. Ma, A. Vrajitoarea, J. Simon, and D. I. Schuster, *Nat. Phys.* **18**, 1048 (2022).
- [34] L. He, Z. Addison, J. Jin, E. J. Mele, S. G. Johnson, and B. Zhen, *Nat. Commun.* **10**, 4194 (2019).
- [35] K. Fang, Z. Yu, and S. Fan, *Nat. Photonics* **6**, 782 (2012).
- [36] I. Chiorescu, P. Bertet, K. Semba, Y. Nakamura, C. J. Harmans, and J. E. Mooij, *Nature (London)* **431**, 159 (2004).